

# Constructing invariant tori using guaranteed Euler method

Jawher Jerry<sup>1</sup> and Laurent Fribourg<sup>2</sup>

<sup>1</sup> Université Sorbonne Paris Nord, LIPN, CNRS, F-93430 Villetaneuse, France  
jerry@lipn.univ-paris13.fr

<sup>2</sup> Université Paris-Saclay, ENS Paris-Saclay, CNRS, LMF, F-91190 Gif-sur-Yvette, France

**Abstract.** We show here how, using Euler’s integration method and an associated function bounding the error in function of time, one can generate structures closely surrounding the invariant tori of dynamical systems. Such structures are constructed from a finite number of balls of  $\mathbb{R}^n$  and encompass the deformations of the tori when small perturbations of the flow of the system occur.

## 1 Introduction

Invariant tori are objects which are omnipresent in physics and intervene in a multiplicity of different domains: chemical reactions, population dynamics, electrical circuit theory, electrodynamics, fluid dynamics, ... (see, e.g., [6,13]). These tori are (positively) *invariant* in the sense that all the orbits lying on their surface at  $t = t_0$  remain on them at all subsequent time  $t \geq t_0$ .

The topology of tori conveys important information. In order to understand it, one introduces a “continuation” parameter (say  $\mu$ ) in the equations of the dynamical system, a simple basic case corresponding to  $\mu = 0$ . One then progressively make  $\mu$  vary, and observe the change of topology of the torus. Roughly speaking, a torus appears when, in a Poincaré section, a stable fixed-point  $M$  becomes unstable while an invariant closed curve (“circle”)  $L$  appears around  $M$ . In the full space,  $M$  corresponds to a *repulsive circle*  $C$  of the system, and  $L$  to an attractive *invariant torus*  $\mathcal{T}$ . Further variations of  $\mu$  lead to the deformation of  $\mathcal{T}$  until a “torus bifurcation” occurs. When  $\mu$  is still modified, the solutions of the system become “aperiodic” and a phenomenon of *chaos* appears.

There are basically three kinds of methods of numerical analysis that exploit this mechanism of parameter continuation: partial differential equation [5,19], graph transform [2,15,16] and orthogonality methods [6,14]. Their respective advantages and disadvantages are analyzed, basically from a computational efficiency point of view, in, e.g., [6,13]. From a formal point of view, all the methods are incomplete because they focus on a *discretization* of the continuous dynamical system, but do not take the associated errors in consideration, or, at best, evaluate them modulo unknown constants (see, e.g., [7,8,15]).

On the other hand, Capinski and co-authors recently developed a *guaranteed* computer assisted method of proof for attractive invariant tori (see [3]). They

obtain an *outer approximation* of the torus via covering by polygons. Their implementation is based on the validated integrators developed by Wilczak and Zgliczynski [20]. We follow a similar approach, but rely here on Euler's integration method associated to an error function  $\delta(t)$  that bounds, at time  $t$ , the distance between the numerical and the exact solutions (see [11]). We are thus able to generate a *finite* number of  $n$ -dimensional balls of radius  $\delta(t)$  for bounded values of  $t$ , which encompass the torus. The set of balls is itself invariant and continues to contain the torus when the latter deforms under small variations of  $\mu$ . This approach extends our previous work [9], which was limited to the determination of invariant circles.

## 2 Preliminaries

### 2.1 Euler's method and error bounds

Let us consider the differential system:

$$\dot{x}(t) = f(x(t)),$$

with states  $x(t) \in \mathbb{R}^n$ . We will use  $x(t; x_0)$  (or sometimes just  $x(t)$ ) to denote the exact continuous solution of the system at time  $t$ , for a given initial condition  $x_0$ . We use  $\tilde{x}(t; y_0)$  (or just  $\tilde{x}(t)$ ) to denote Euler's approximate value of  $x(t; y_0)$  (defined by  $\tilde{x}(t; y_0) = y_0 + tf(y_0)$  for  $t \in [0, \tau]$ , where  $\tau$  is the integration time-step).

We suppose that we know a bounded region  $\mathcal{S} \subset \mathbb{R}^n$  containing the solutions of the system for a set of initial conditions  $B_0$  and a certain amount of time. We now give an upper bound to the error between the exact solution of the ODE and its Euler approximation on  $\mathcal{S}$  (see [11]).

**Definition 1.** Let  $\varepsilon$  be a given positive constant. Let us define, for  $t \in [0, \tau]$ ,  $\delta_\varepsilon(t)$  as follows:  
if  $\lambda < 0$  :

$$\delta_\varepsilon(t) = \left( \varepsilon^2 e^{\lambda t} + \frac{C^2}{\lambda^2} \left( t^2 + \frac{2t}{\lambda} + \frac{2}{\lambda^2} (1 - e^{\lambda t}) \right) \right)^{\frac{1}{2}}$$

if  $\lambda = 0$  :

$$\delta_\varepsilon(t) = \left( \varepsilon^2 e^t + C^2(-t^2 - 2t + 2(e^t - 1)) \right)^{\frac{1}{2}}$$

if  $\lambda > 0$  :

$$\delta_\varepsilon(t) = \left( \varepsilon^2 e^{3\lambda t} + \frac{C^2}{3\lambda^2} \left( -t^2 - \frac{2t}{3\lambda} + \frac{2}{9\lambda^2} (e^{3\lambda t} - 1) \right) \right)^{\frac{1}{2}}$$

where  $C$  and  $\lambda$  are real constants specific to function  $f$ , defined as follows:

$$C = \sup_{y \in \mathcal{S}} L \|f(y)\|,$$

where  $L$  denotes the Lipschitz constant for  $f$ , and  $\lambda$  is the “one-sided Lipschitz constant” (or “logarithmic Lipschitz constant” [1]) associated to  $f$ , i. e., the minimal constant such that, for all  $y_1, y_2 \in \mathcal{S}$ :

$$\langle f(y_1) - f(y_2), y_1 - y_2 \rangle \leq \lambda \|y_1 - y_2\|^2, \quad (H0)$$

where  $\langle \cdot, \cdot \rangle$  denotes the scalar product of two vectors of  $\mathcal{S}$  and  $\|\cdot\|$  the Euclidean norm.

The constant  $\lambda$  can be computed using a nonlinear optimization solver (e. g., CPLEX [4]) or using the Jacobian matrix of  $f$  (see, e. g., [1]).

## 2.2 Systems with bounded uncertainty

Let us now show how the method extends to systems with “disturbance” or “bounded uncertainty”. A differential system  $\Sigma_{\mathcal{W}}$  with bounded uncertainty is of the form

$$\dot{x}(t) = f(x(t), w(t)),$$

with  $t \in \mathbb{R}_{\geq 0}^n$ , states  $x(t) \in \mathbb{R}^n$ , and uncertainty  $w(t) \in \mathcal{W} \subset \mathbb{R}^n$  ( $\mathcal{W}$  is compact, i. e., closed and bounded). We assume that any possible disturbance trajectory is bounded at any point in time in the compact set  $W$ . We denote this by  $w \in \mathcal{W}$ , which is a shorthand for  $w(t) \in \mathcal{W}, \forall t \geq 0$ . See [18, 17] for details. We now suppose (see [10]) that there exist constants  $\lambda \in \mathbb{R}$  and  $\gamma \in \mathbb{R}_{\geq 0}$  such that, for all  $y_1, y_2 \in \mathcal{S}$  and  $w_1, w_2 \in \mathcal{W}$ :

$$\begin{aligned} & \langle f(y_1, w_1) - f(y_2, w_2), y_1 - y_2 \rangle \\ & \leq \lambda \|y_1 - y_2\|^2 + \gamma \|y_1 - y_2\| \|w_1 - w_2\| \end{aligned} \quad (H1).$$

This formula can be seen as a generalization of (H0) (see Section 2.1). Recall that  $\lambda$  has to be computed in the absence of uncertainty ( $\mathcal{W} = 0$ ). The additional constant  $\gamma$  is used for taking into account the uncertainty  $w$ . Given  $\lambda$ , the constant  $\gamma$  can be computed itself using a nonlinear optimization solver (e. g., CPLEX [4]). We now give a property originally proved in [10].

**Proposition 1.** [10] *Consider a system  $\Sigma_{\mathcal{W}}$  with bounded uncertainty of the form  $\dot{x}(t) = f(x(t), w(t))$  satisfying (H1). Consider a point  $x_0 \in \mathcal{S}$  and a point  $y_0 \in B(x_0, \varepsilon)$ <sup>3</sup>. Let  $x(t; y_0)$  be the exact solution of  $\Sigma_{\mathcal{W}}$  with bounded uncertainty  $\mathcal{W}$  and initial condition  $y_0$ , and  $\tilde{x}(t; x_0)$  the Euler approximate solution of the system  $\Sigma_0 : \dot{x}(t) = f(x(t), 0)$  without uncertainty ( $\mathcal{W} = 0$ ) with initial condition  $x_0$ . We have, for all  $w \in \mathcal{W}$  and  $t \in [0, \tau]$ :*

$$\|x(t; y_0) - \tilde{x}(t; x_0)\| \leq \delta_{\varepsilon, \mathcal{W}}(t)$$

with

---

<sup>3</sup> As usual,  $B(x_0, \varepsilon)$  denotes the ball of center  $x_0$  and radius  $\varepsilon$  defined by  $B(x_0, \varepsilon) := \{x' \in \mathcal{S} \mid \|x_0 - x'\| \leq \varepsilon\}$ .

– if  $\lambda < 0$ ,

$$\begin{aligned} \delta_{\varepsilon, \mathcal{W}}(t) = & \left( \frac{C^2}{-\lambda^4} (-\lambda^2 t^2 - 2\lambda t + 2e^{\lambda t} - 2) \right. \\ & + \frac{1}{\lambda^2} \left( \frac{C\gamma|\mathcal{W}|}{-\lambda} (-\lambda t + e^{\lambda t} - 1) \right. \\ & \left. \left. + \lambda \left( \frac{\gamma^2(|\mathcal{W}|/2)^2}{-\lambda} (e^{\lambda t} - 1) + \lambda \varepsilon^2 e^{\lambda t} \right) \right) \right)^{1/2} \end{aligned} \quad (1)$$

where  $|\mathcal{W}|$  denotes the maximum distance between two elements of  $\mathcal{W}$ .

– if  $\lambda > 0$ ,

$$\begin{aligned} \delta_{\varepsilon, \mathcal{W}}(t) = & \frac{1}{(3\lambda)^{3/2}} \left( \frac{C^2}{\lambda} (-9\lambda^2 t^2 - 6\lambda t + 2e^{3\lambda t} - 2) \right. \\ & + 3\lambda \left( \frac{C\gamma|\mathcal{W}|}{\lambda} (-3\lambda t + e^{3\lambda t} - 1) \right. \\ & \left. \left. + 3\lambda \left( \frac{\gamma^2(|\mathcal{W}|/2)^2}{\lambda} (e^{3\lambda t} - 1) + 3\lambda \varepsilon^2 e^{3\lambda t} \right) \right) \right)^{1/2} \end{aligned} \quad (2)$$

– if  $\lambda = 0$ ,

$$\begin{aligned} \delta_{\varepsilon, \mathcal{W}}(t) = & (C^2 (-t^2 - 2t + 2e^t - 2) \\ & + (C\gamma|\mathcal{W}| (-t + e^t - 1) \\ & + (\gamma^2(|\mathcal{W}|/2)^2 (e^t - 1) + \varepsilon^2 e^t)))^{1/2} \end{aligned} \quad (3)$$

We will sometimes write  $\delta_{\mathcal{W}}(t)$  instead of  $\delta_{\varepsilon, \mathcal{W}}(t)$ .

Actually, we will not compute  $\lambda$  (resp.  $\gamma$ ) *globally* for  $\mathcal{S}$ , but will decompose  $\mathcal{S}$  into a set of subregions  $\{\mathcal{S}_i\}_{i=1, \dots, k}$  with  $k\tau = T$ , where  $\mathcal{S}_i$  is an appropriate subregion of  $\mathcal{S}$  enclosing the states of the system state during the interval of time  $[(i-1)\tau, i\tau]$ . Instead of a global upperbound of  $\lambda$  satisfying (H1) on  $\mathcal{S}$ , we will compute a *local* upperbound  $\lambda_i$  (resp.  $\gamma_i$ ) of  $\lambda$  (resp.  $\gamma$ ) on each subregion  $\mathcal{S}_i$  ( $1 \leq i \leq k$ ). [Proposition 1](#) extends naturally in this context.

### 3 Constructing Invariant Structures Around Tori

Consider a differential system  $\Sigma_{\mathcal{W}} : \dot{x} = f(x, w)$  with  $w \in \mathcal{W}$ , an initial point  $x_0 \in \mathbb{R}^n$ , a real  $\varepsilon > 0$  and a ball  $B_0 = B(x_0, \varepsilon)$ . Let  $\mathcal{B}_{\varepsilon, \mathcal{W}}(t)$  denote  $B(\tilde{x}(t), \delta_{\varepsilon, \mathcal{W}}(t))$  where  $\tilde{x}(t)$  is the Euler approximate solution of the system without uncertainty and initial condition  $x_0$ <sup>4</sup>. It follows from [Proposition 1](#) that  $\bigcup_{t \geq 0} \mathcal{B}_{\varepsilon, \mathcal{W}}(t)$  is an invariant set containing  $B_0$ . We can make a stroboscopic map of this invariant. by considering periodically the set  $\mathcal{B}_{\varepsilon, \mathcal{W}}(t)$  at the moments  $t = 0, T, 2T$ , etc., with  $T = k\tau$  for some  $k$  ( $\tau$  is the time-step used in

<sup>4</sup> Note that  $\mathcal{B}_{\varepsilon, \mathcal{W}}(0) = B_0$  because  $\tilde{x}(0) = x_0$  and  $\delta_{\varepsilon, \mathcal{W}}(0) = \varepsilon$ .

Euler's method). The value of  $T$  is an estimate of the exact period  $T^*$  of the system.

If moreover, we can find an integer  $i \geq 0$  such that  $\mathcal{B}_{\varepsilon, \mathcal{W}}((i+1)T) \subseteq \mathcal{B}_{\varepsilon, \mathcal{W}}(iT)$ , then we have  $\mathcal{B}_{\varepsilon, \mathcal{W}}(iT) = \bigcup_{j=i, i+1, \dots} \mathcal{B}_{\varepsilon, \mathcal{W}}(jT)$  and  $\bigcup_{t \in [0, (i+1)T]} \mathcal{B}_{\varepsilon, \mathcal{W}}(t) = \bigcup_{t \geq 0} \mathcal{B}_{\varepsilon, \mathcal{W}}(t)$ . The set  $\bigcup_{t \in [0, (i+1)T]} \mathcal{B}_{\varepsilon, \mathcal{W}}(t)$  is thus a *bounded invariant* which contains all the solutions  $x(t)$  starting at  $B_0$ , for  $t \in [0, \infty)$ . We have:

**Proposition 2.** [9] *Consider a system  $\Sigma_{\mathcal{W}} : \dot{x} = f(x, w)$  with uncertainty  $w \in \mathcal{W}$  satisfying (H1), and a set of initial conditions  $B_0 \equiv B(x_0, \varepsilon)$ . Suppose that there exist  $T > 0$  (with  $T = k\tau$  for some  $k \in \mathbb{N}$ ) and  $i \in \mathbb{N}$  such that*

$$(*) : \mathcal{B}_{\varepsilon, \mathcal{W}}((i+1)T) \subseteq \mathcal{B}_{\varepsilon, \mathcal{W}}(iT).$$

*Then we have:*

1.  $\bigcup_{t \in [0, (i+1)T]} \mathcal{B}_{\varepsilon, \mathcal{W}}(t)$  is a compact (i.e., bounded and closed) invariant set containing, for  $t \in [0, \infty)$ , all the solutions  $x(t)$  of  $\Sigma_{\mathcal{W}}$  with initial condition in  $B_0$ .
2. The subset  $\bigcup_{t \in [iT, (i+1)T]} \mathcal{B}_{\varepsilon, \mathcal{W}}(t)$  contains an attractive circle (or “stable limit cycle”) of the system  $\Sigma_0$  without uncertainty ( $w = 0$ ).

Proposition 2 states that the invariant set  $\bigcup_{t \in [0, (i+1)T]} \mathcal{B}_{\varepsilon, \mathcal{W}}(t)$  is an  $n$ -dimensional tube having the form of a “lasso” composed of a linear part  $\bigcup_{t \in [0, iT]} \mathcal{B}_{\varepsilon, \mathcal{W}}(t)$  connected to a looping part  $\bigcup_{t \in [iT, (i+1)T]} \mathcal{B}_{\varepsilon, \mathcal{W}}(t)$ . Besides, the looping part encloses a 1-dimensional attractive circle. Since  $\mathcal{B}_{\varepsilon, \mathcal{W}}(t)$  is a ball of  $\mathbb{R}^n$  (of radius  $\delta_{\varepsilon, \mathcal{W}}(t)$ ), a lasso is constructed from a *finite* number (*viz.*,  $(i+1) \times k$ ) of balls.

Given  $\varepsilon, \mathcal{W}, \tau, T = k\tau$ , the lasso:  $\bigcup_{t \in [0, (i+1)T]} \mathcal{B}_{\varepsilon, \mathcal{W}}(t)$  is uniquely determined by the center  $x_0 \in \mathbb{R}^n$  of the initial ball  $B_0 = B(x_0, \varepsilon)$  and by  $i_0$ , the integer such that  $(*)$  holds. We call  $x_0$  the *source point* of the lasso, and  $B_0 = B(x_0, \varepsilon)$  the source ball. We will denote such a lasso by  $\mathcal{L}(x_0, i_0)$  or more simply by  $\mathcal{L}(x_0)$ , where  $i_0$  is left implicit. Note that the invariance property of a lasso  $\mathcal{L}(x_0)$  is *robust*: the invariance persists even in presence of a bounded perturbation  $w \in \mathcal{W}$  of the dynamical system.

The implementation of the construction of lassos has been done in Python and corresponds to a program of around 500 lines. The source code is available at [lipn.univ-paris13.fr/~jerray/orbitador/](http://lipn.univ-paris13.fr/~jerray/orbitador/). In the experiments below, the program runs on a 2.80 GHz Intel Core i7-4810MQ CPU with 8 GiB of memory. Given  $x_0$ , one searches for values of  $\tau, \varepsilon, \mathcal{W}, T$  at hand (by trial and error) so that inclusion  $(*)$  can be successfully verified by the program.

*Example 1.* Consider the forced Van der Pol (VdP) system  $\Sigma_{\mathcal{W}}$  with initial condition in  $B_0 = B(x_0, \varepsilon)$  for some  $x_0 \in \mathbb{R}^3$  and  $\varepsilon > 0$  (adapted from [13]).

$$\begin{aligned} \dot{x}_1 &= \frac{x_1(\sqrt{x_1^2 + x_2^2} - 3)}{\sqrt{x_1^2 + x_2^2}} (\mu - (\sqrt{x_1^2 + x_2^2} - 3)^2 - x_3^2) - \frac{x_2^2 + x_1 x_3}{\sqrt{x_1^2 + x_2^2}} + w \\ \dot{x}_2 &= \frac{x_2(\sqrt{x_1^2 + x_2^2} - 3)}{\sqrt{x_1^2 + x_2^2}} (\mu - (\sqrt{x_1^2 + x_2^2} - 3)^2 - x_3^2) + \frac{x_1 x_2 - x_2 x_3}{\sqrt{x_1^2 + x_2^2}} + w \\ \dot{x}_3 &= (\sqrt{x_1^2 + x_2^2} - 3) + \mu x_3 - x_3((\sqrt{x_1^2 + x_2^2} - 3)^2 + x_3^2) + w \end{aligned}$$

with a parameter  $\mu$  that controls the periodic forcing term and a bounded perturbation  $w \in \mathcal{W}$ . Here  $\mu = 1$  and  $\mathcal{W} = [-0.001, 0.001]$ . Let the time-step be

equal to  $\tau = 10^{-3}$  and the radius of the initial ball around the source points be  $\varepsilon = 0.05$ . Let  $T = 6.283$  be used as an approximation of the exact period  $T^* = 2\pi$  of the system. Let  $X(t) := (x_1(t), x_2(t), x_3(t))$  with source point  $X(0) := (4, -10^{-3}, -4.8985872 \cdot 10^{-16})$  and  $\delta_{\mathcal{W}}(0) = \varepsilon = 0.05$ . We have:

$$\begin{aligned} X(T) &= (3.96480714, -5.31384851 \cdot 10^{-1}, -1.78122434 \cdot 10^{-4}), \delta_{\mathcal{W}}(T) = 0.009369013554590614 \\ X(2T) &= (-3.99399126, -2.23716163 \cdot 10^{-1}, -1.12718456 \cdot 10^{-3}), \delta_{\mathcal{W}}(2T) = \\ &0.013528832294010595 \\ X(3T) &= (-4.00024909, -4.16869048 \cdot 10^{-4}, -1.31261670 \cdot 10^{-3}), \delta_{\mathcal{W}}(3T) = \\ &0.008339289838071407 \\ X(4T) &= (-4.00024885, -7.76179315 \cdot 10^{-7}, -1.49692259 \cdot 10^{-3}), \delta_{\mathcal{W}}(4T) = \\ &0.008181686420182348 \\ X(5T) &= (-4.00024856, -1.44518842 \cdot 10^{-9}, -1.68122843 \cdot 10^{-3}), \delta_{\mathcal{W}}(5T) = \\ &0.008088285030977036 \\ X(6T) &= (-4.00024823, -2.69083383 \cdot 10^{-12}, -1.86553421 \cdot 10^{-3}), \delta_{\mathcal{W}}(6T) = \\ &0.008001319005309636 \\ X(7T) &= (-4.00024787, -5.01013330 \cdot 10^{-15}, -2.04983993 \cdot 10^{-3}), \delta_{\mathcal{W}}(7T) = \\ &0.008408806943539475 \\ X(8T) &= (-4.00024747, -9.32849705 \cdot 10^{-18}, -2.23414558 \cdot 10^{-3}), \delta_{\mathcal{W}}(8T) = \\ &0.007976450475139826. \end{aligned}$$

We have:  $\mathcal{B}_{\mathcal{W}}(8T) \subset \mathcal{B}_{\mathcal{W}}(7T)$ , i.e.:  $\mathcal{B}_{\mathcal{W}}((i_0 + 1)T) \subset \mathcal{B}_{\mathcal{W}}(i_0T)$  for  $i_0 = 7$ . The computation takes 1038 seconds of CPU time. See Fig. 1. An analogous computation of lassos for 3 other source points takes 4052 seconds. The 4 lassos are depicted together on Fig. 2.

Given a closed orbit (“circle”)  $C$ , and a union  $\mathcal{R}$  of balls of radius  $\varepsilon > 0$ , we say that  $\mathcal{R}$  *isolates*  $C$  if there exists  $\alpha > 0$  such that:

(\*\*) Any continuous curve containing a point of  $C$  and a point located at distance  $\alpha$  from  $C$ , also contains a point of  $\mathcal{R}$ .

We say that  $\mathcal{R}$  is at distance  $\alpha_0 > 0$  of  $C$ , where  $\alpha_0$  is the greatest  $\alpha$  satisfying property (\*\*).

Let  $\mathcal{T}$  be a torus of repulsive circle  $C$ , and  $\mathcal{M}$  a set of lassos. We say that  $\mathcal{M}$  *covers*  $\mathcal{T}$  (besides the  $\alpha_0$ -neighborhood of  $C$ ), if all orbit  $\mathcal{O}$  on  $\mathcal{T}$  starting at a distance greater than  $\alpha_0$  from  $C$  is contained in a lasso of  $\mathcal{M}$ . We have:

**Theorem 1.** *Let  $\mathcal{T}$  be a torus of repulsive circle  $C$ , and  $\mathcal{R}$  a union of balls of  $\mathbb{R}^n$  isolating  $C$  at distance  $\alpha_0$ . The set of lassos  $\mathcal{M}$  having the balls of  $\mathcal{R}$  as source balls, covers  $\mathcal{T}$  (besides the  $\alpha_0$ -neighborhood of  $C$ ). Furthermore,  $\mathcal{M}$  continues to cover  $\mathcal{T}$  for a bounded perturbation  $w \in \mathcal{W}$  of the dynamical system.*

The proof is based on the fact that, by Proposition 2, each lasso of  $\mathcal{M}$  connects its source ball to an attractive circle. (The full proof will be given in the long version of this paper.) Note that the application of Theorem 1 requires the prior estimate of the location of the torus repulsive circle  $C$ . Actually, as seen in the forthcoming examples, taking a subset  $\mathcal{R}'$  of  $\mathcal{R}$  as source balls, even if  $\mathcal{R}'$  does not isolate  $C$  “completely”, suffices to provide useful information on  $\mathcal{T}$ .

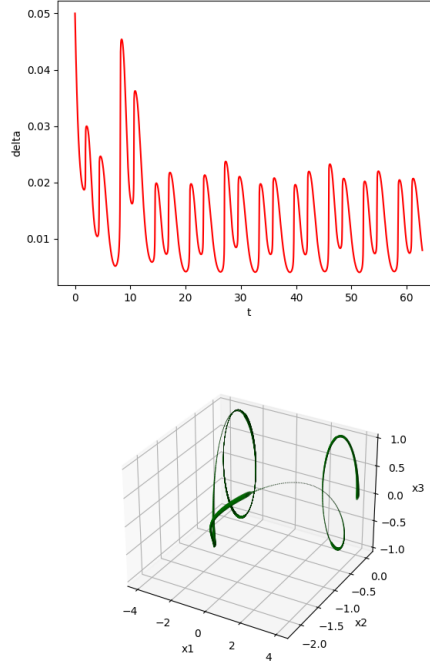


Fig. 1: *Forced VdP*. Top: the function  $\delta_{\mathcal{W}}(t)$  giving the evolution of the radius of a lasso ball. Bottom: the corresponding invariant lasso.

*Example 2.* For the system of [Example 1](#), we generate 100 lassos which (partially) cover the invariant torus of the system, as depicted on [Fig. 3](#). The choice of the 100 source points is as follows. One knows (see [\[13\]](#)) that the system has, in the  $x_2$ - $x_3$  plane, a *repulsive* invariant circle  $C$  of centre  $(3, 0, 0)$  and radius 1. We thus take 100 source points distributed in the vicinity of the circumference of  $C$ . The same values of  $\varepsilon, \tau, T = k\tau, \mathcal{W}$  are used for all the lassos (see [Example 1](#)). For each source point, the generation of the corresponding lasso stops when the inclusion relation (\*) is verified, which takes around 1000 seconds of CPU time<sup>5</sup>. Note that, as stated by [Proposition 2](#), the looping part of each lasso contains an *attractive* invariant circle (here, the circle of centre  $(-3, 0, 0)$  and radius 1, in the  $x_2$ - $x_3$  plane).

An other example (coupled VdP oscillators) is given in Appendix.

<sup>5</sup> which means a total of nearly 30 hours of CPU time for generating the 100 lassos.

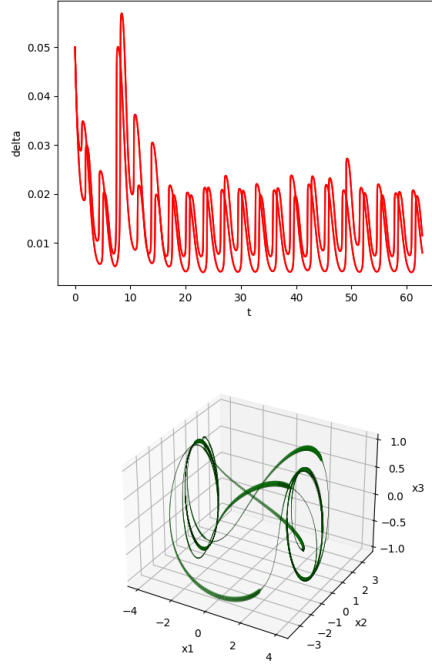


Fig. 2: *Forced VdP*. Top: the function  $\delta_W(t)$  giving the evolution of the radius of 4 lasso balls. Bottom: the 4 corresponding invariant lassos.

## 4 Final Remarks

We have introduced a simple technique based on Euler’s integration method which allows us to construct an invariant structure made of a finite number of  $n$ -dimensional balls covering the invariant torus of the system. Although it has not been done here, the implementation can be fully parallelized since the construction of each lasso is independent of each other. We have shown on a 3D and a 4D example (one of them close to a torus bifurcation) how our method gives *guaranteed* information on the torus topology. Such a method, which takes into account the discretization errors, can help to complement the results obtained with standard numerical methods.

## References

1. Aminzare, Z., Sontag, E.D.: Contraction methods for nonlinear systems: A brief introduction and some open problems. In: 53rd IEEE Conference on Decision and Control, CDC 2014, Los Angeles, CA, USA, December 15-17, 2014. pp. 3835–3847 (2014)



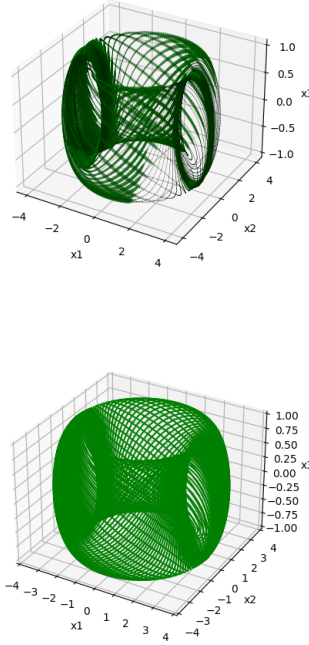


Fig. 3: *Forced VdP*. A set of 50 lassos (top) and 100 lassos (bottom) partially covering the invariant torus.

2. Broer, H., Hagen, A., Vegter, G.: Numerical approximation of normally hyperbolic invariant manifolds (2002)
3. Capinski, M.J., Fleurantin, E., Mireles James, J.D.: Computer Assisted Proofs of Attracting Invariant Tori for ODEs. arXiv e-prints arXiv:1905.08116 (May 2019)
4. Cplex, I.I.: V12. 1: User's manual for cplex. International Business Machines Corporation **46**(53), 157 (2009)
5. Dieci, L., Bader, G.: Solution of the systems associated with invariant tori approximation. II: multigrid methods. SIAM J. Sci. Comput. **15**(6), 1375–1400 (1994). <https://doi.org/10.1137/0915083>, <https://doi.org/10.1137/0915083>
6. Edoh, K.D., Russell, R.D., Sun, W.: Computation of invariant tori by orthogonal collocation. Appl. Numer. Math. **32**(3), 273–289 (Mar 2000). [https://doi.org/10.1016/S0168-9274\(99\)00029-X](https://doi.org/10.1016/S0168-9274(99)00029-X), [https://doi.org/10.1016/S0168-9274\(99\)00029-X](https://doi.org/10.1016/S0168-9274(99)00029-X)
7. Garay, B.: Estimates in discretizing normally hyperbolic compact invariant manifolds of ordinary differential equations. Computers & Mathematics With Applications **42**, 1103–1122 (2001)
8. Hairer, E., Lubich, C.: Invariant tori of dissipatively perturbed hamiltonian systems under symplectic discretization. Appl. Numer. Math. **29**(1), 57–71 (Jan 1999)
9. Jerray, J., Fribourg, L.: Determination of limit cycles using stroboscopic set-valued maps. In: Jungers, R. (ed.) 7th IFAC Conference on Analysis and Design of Hy-

- brid Systems, ADHS 2021, Brussels, Belgium, July 7-9, 2021. IFAC-PapersOnLine, Elsevier (2021)
10. Le Coënt, A., Alexandre Dit Sandretto, J., Chapoutot, A., Fribourg, L., De Vuyst, F., Chamoin, L.: Distributed control synthesis using Euler’s method. In: Proc. of International Workshop on Reachability Problems (RP’17). Lecture Notes in Computer Science, vol. 247, pp. 118–131. Springer (2017)
  11. Le Coënt, A., De Vuyst, F., Chamoin, L., Fribourg, L.: Control synthesis of nonlinear sampled switched systems using Euler’s method. In: Proc. of International Workshop on Symbolic and Numerical Methods for Reachability Analysis (SNR’17). EPTCS, vol. 247, pp. 18–33. Open Publishing Association (2017)
  12. Moore, G.: Computation and parametrisation of invariant curves and tori. SIAM Journal on Numerical Analysis **33**, 2333–2358 (1996)
  13. Rasmussen, B.: Numerical methods for the continuation of invariant tori (2003)
  14. Rasmussen, B., Dieci, L.: A geometrical method for the approximation of invariant tori. J. Comput. Appl. Math. **216**(2), 388–412 (Jun 2008). <https://doi.org/10.1016/j.cam.2007.05.025>, <https://doi.org/10.1016/j.cam.2007.05.025>
  15. Reichelt, V.: Computing invariant tori and circles in dynamical systems. In: Doedel, E., Tuckerman, L.S. (eds.) Numerical Methods for Bifurcation Problems and Large-Scale Dynamical Systems. pp. 407–437. Springer New York, New York, NY (2000)
  16. Schilder, F., Osinga, H., Vogt, W.: Continuation of quasi-periodic invariant tori. SIAM Journal on Applied Dynamical Systems **4** (3), 459 – 488 (Jan 2005). <https://doi.org/10.1137/040611240>, publisher: Society for Industrial and Applied Mathematics
  17. Schürmann, B., Althoff, M.: Guaranteeing constraints of disturbed nonlinear systems using set-based optimal control in generator space. IFAC-PapersOnLine **50**(1), 11515 – 11522 (2017). <https://doi.org/https://doi.org/10.1016/j.ifacol.2017.08.1617>, <http://www.sciencedirect.com/science/article/pii/S2405896317322152>, 20th IFAC World Congress
  18. Schürmann, B., Althoff, M.: Optimal control of sets of solutions to formally guarantee constraints of disturbed linear systems. In: 2017 American Control Conference, ACC 2017, Seattle, WA, USA, May 24-26, 2017. pp. 2522–2529 (2017). <https://doi.org/10.23919/ACC.2017.7963332>
  19. Trummer, M.R.: Spectral methods in computing invariant tori. Appl. Numer. Math. **34**(2–3), 275–292 (Jul 2000). [https://doi.org/10.1016/S0168-9274\(99\)00133-6](https://doi.org/10.1016/S0168-9274(99)00133-6), [https://doi.org/10.1016/S0168-9274\(99\)00133-6](https://doi.org/10.1016/S0168-9274(99)00133-6)
  20. Wilczak, D., Zgliczyński, P.:  $C^r$ -Lohner algorithm. arXiv e-prints arXiv:0704.0720 (Apr 2007)

## Appendix: Coupled VdP Oscillators Example

*Example 3.* Consider the system of coupled VdP oscillators described in [6]:

$$\begin{cases} \dot{\theta}_1 = \beta_1 + \mu \left\{ \cos 2\theta_1 - \frac{r_2}{r_1} [\sin(\theta_1 - \theta_2) + \cos(\theta_1 + \theta_2)] \right\} + w \\ \dot{\theta}_2 = \beta_2 + \mu \left\{ \cos 2\theta_2 - \frac{r_1}{r_2} [\sin(\theta_2 - \theta_1) + \cos(\theta_1 + \theta_2)] \right\} + w \\ \dot{r}_1 = r_1(\alpha_1 - r_1^2) + \mu \{r_1(1 - \sin 2\theta_1) + Ar_2\} + w \\ \dot{r}_2 = r_2(\alpha_1 - r_2^2) + \mu \{r_2(1 - \sin 2\theta_2) + Ar_1\} + w \end{cases} \quad (4)$$

where  $A = \sin(\theta_1 + \theta_2) - \cos(\theta_1 - \theta_2)$ .

The parameter  $\mu$  is the coupling constant and the oscillators decouple for  $\mu = 0$ . Each oscillator has then a unique attractive circle, and the uncoupled product system has a unique attractive invariant torus. The torus persists for a weak coupling and contains two periodic circles, one is attractive and the other is repulsive when  $\beta_1 = \beta_2$  (see [6] for details). If the manifold  $M = (\theta_1, \theta_2, r_1(\theta_1, \theta_2), r_2(\theta_1, \theta_2))$  denotes an invariant torus for the system, then the uncoupled system has an invariant torus defined by  $M_1 := (\theta_1, \theta_2, 1, 1)$ .

Here, we take  $w \in \mathcal{W} = [-0.0001, 0.0001]$  and, as in [6],  $\alpha_1 = \alpha_2 = 1.0$ ,  $\beta_1 = \beta_2 = \beta = 0.55$ , and  $\mu = 0.2601$ . Let the time-step  $\tau = 10^{-3}$ , and the radius of the initial ball around the source points  $\varepsilon = 0.1$ . Let  $T = 11.425$  be used as an approximation of the exact period  $T^* = \frac{2\pi}{\beta}$ . Each lasso generation now takes around 35 minutes of CPU time. We focus visually on the representation of the projections  $r_1(\theta_1, \theta_2)$  and  $r_2(\theta_1, \theta_2)$ . Ten simulations are thus depicted on Figs. 4 and 5, and the corresponding lassos on Figs. 6 and 7. The value of  $\mu$  is close to the value  $\mu_1 \approx 0.2605$  for which a torus bifurcation appears (see [6]; cf [5,12]). This explains the extent of the deformation of the structure, the attractive circle being shaped like a eight figure on Figs. 4 and 5. The source points of the 10 lassos (which coincide with the initial points of the simulations) have been chosen close to the repulsive circle (itself estimated by numerical simulation), as follows:

$$\begin{aligned} X(0) &= (0, 3.14159265, 1.05980274, 1.02028354) \\ X(0) &= (0.62831853, 3.76991118, 0.95715177, 1.08632695) \\ X(0) &= (1.25663706, 4.39822972, 1.03960697, 0.93217529) \\ X(0) &= (1.88495559, 5.02654825, 0.99657, 1.09545089) \\ X(0) &= (2.51327412, 5.65486678, 1.02811851, 1.0178553) \\ X(0) &= (3.14159265, 0, 1.08476381, 0.97121437) \\ X(0) &= (3.76991118, 0.62831853, 0.97369993, 0.93966289) \\ X(0) &= (4.39822972, 1.25663706, 1.05513594, 1.00555761) \\ X(0) &= (5.02654825, 1.88495559, 0.98407245, 1.09722914) \\ X(0) &= (5.65486678, 2.51327412, 0.98484401, 0.93636707). \end{aligned}$$

For each source point, the inclusion relation (\*) is checked for  $i = 3, 4$  or  $5$ .

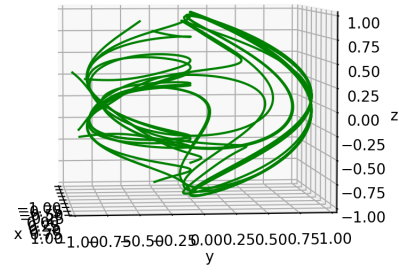
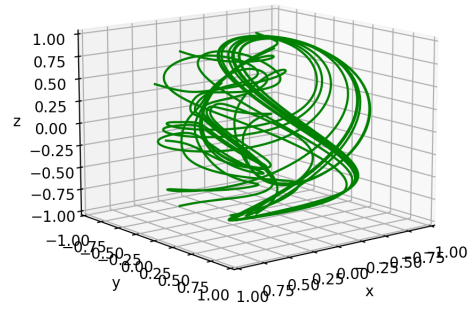


Fig. 4: *Coupled VdP*. The function  $r_1(\theta_1, \theta_2)$  corresponding to 10 simulations, under two different views.

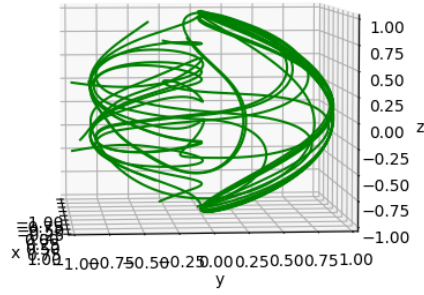
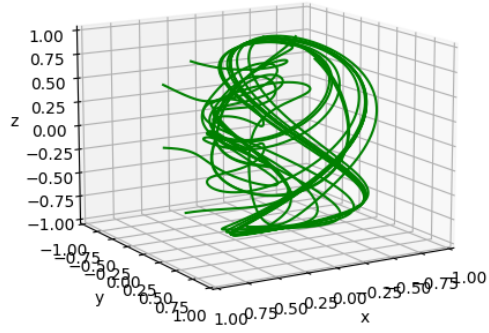


Fig. 5: *Coupled VdP*. The function  $r_2(\theta_1, \theta_2)$  corresponding to 10 simulations, under two different views.

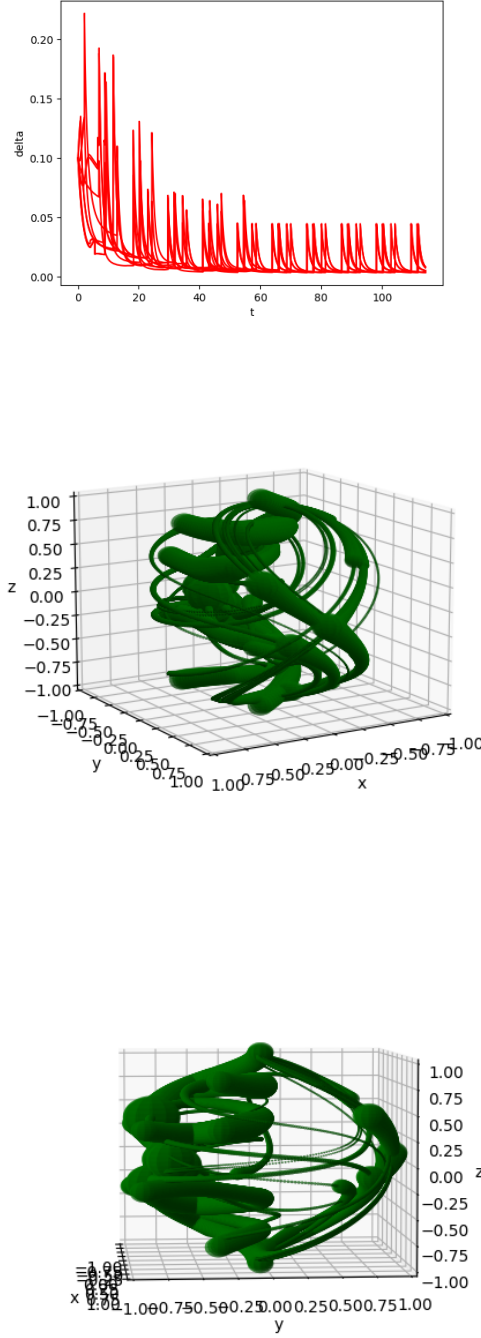


Fig. 6: *Coupled VdP*. Middle and bottom: The function  $r_1(\theta_1, \theta_2)$  corresponding to the lassos associated with the 10 simulations of Fig. 4, under the same views. Top: the radius  $\delta_W(t)$  of these lassos.

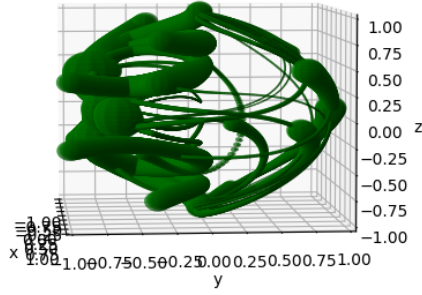
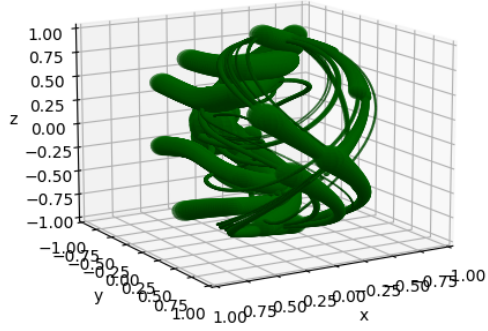


Fig. 7: *Coupled VdP*. Top and bottom: The function  $r_2(\theta_1, \theta_2)$  corresponding to the lassos associated with the 10 simulations of Fig. 5, under the same views.